RSC Advances

ROYAL SOCIETY
OF **CHEMISTRY**

www.rsc.org/advances

Journal Name

ARTICLE

Ripening and Recrystallization of NaCl Nanocrystals in Humid Conditions

M. Oliva-Ramirez[1], M. Macías-Montero[1,2], A. Borras[1], A.R. González-Elipe[1*]

This work shows that Ostwald ripening, a universal mechanism responsible for the increase of crystal size during precipitation from solutions, can be meditated by ion diffusion through condensed monolayers of water connecting separated nanocrystals. In an environmental electron microscope we have observed "in-situ" the time evolution of the number, shape, size and crystallographic texture of NaCl nanoparticles deposited by electron beam evaporation at oblique angles. Analysis of NaCl nanoparticles before and after water vapor condensation has evidenced that the size of nanocrystals is not the unique driving force inducing nanoparticle ripening and recrystallization but also the faceting of their crystalline habits and the amorphisation degree of the initially deposited nuclei. These findings have implications for other crystallization and nucleation processes and can be of relevance for rock weathering and related phenomena.

Introduction

Ostwald ripening is a universal coarsening phenomenon occurring during crystallization in solutions[1–3] and in other systems such as water droplets[4,5] or emulsions[6] that leads to the size increase of nuclei bigger than a critical value (i.e. critical nucleation size dc) at expenses of those with a smaller size[7]. This phenomenon has been recursively studied at fundamental level[2,8–14] and technologically applied to control the crystal size distribution in precipitates, tune the hollow microstructure of nanostructured materials or to grow nanostructures with well selected sizes and shapes[15–17]. According to the original proposals of Ostwald[18], ripening is driven by the size dependence of the surface to bulk energy ratio and requires a dispersive medium enabling material diffusion among nuclei.

In nature, geological precipitation of crystals[19,20], rock weathering[21] or ice formation in the troposphere[22] can be mediated by Ostwald ripening after the dissolution of salt precipitates in rain or surface condensed water. Dissolution phenomena looking to the effect of condensed layers of water on single crystals and other model systems have been monitored "in situ" by AFM23, environmental XPS[23–25] or TEM[26]. Herein, the ripening process occurring in a multi-nuclei NaCl system has been directly monitored inside an Environmental Scanning Electron Microscope (ESEM) where water vapour pressure was increased up to saturation. Under these conditions, we followed the time evolution of the number, size and shapes of the salt nanoparticles and found some un-expected clues determining their transformation. This "in situ" ESEM investigation has been complemented with "in-situ" and "ex-situ" X-ray diffraction analysis to verify possible modifications in crystalline

structure. For this study we have electron beam evaporated NaCl in an oblique angle deposition (OAD) configuration (also known as glancing angle deposition, GLAD) [27,28] onto Si(100) wafer substrates. This geometrical arrangement offers invaluable possibilities of microstructure control that had not been explored before with NaCl, even if thin films of this material has been recurrently deposited by physical vapour deposition in a normal configuration[29–31]. Evaporation at oblique angles promotes the appearance of shadowing effects during deposition and leads to the initial formation of isolated nuclei and the subsequent growth of thin films with an open and tilted columnar nanostructure[27,28, 32,33]. By controlling different deposition parameters, particularly the zenithal angle of deposition (i.e., angle formed between the NaCl evaporated flux and the perpendicular to the substrate surface), we have been able to control the size, shape and connectivity of the initially formed NaCl nuclei. Ripening results will be shown for selected samples deposited at zenithal angles of 60º and 85º (hereafter named as NaCl-60º and NaCl-85º).

Results and Discussion

Nanoparticle morphology and crystallographic structure

Figure 1 shows a series of normal SEM images and the XRD diagrams recorded for NaCl-60º and -85º "as-prepared" samples. In the former, the salt nanoparticles appear interconnected and present rounded edged profiles, while its diffraction diagram taken in a Bragg-Brentano configuration reveals a texture where the (220) planes are parallel to the substrate surface. By contrast, the NaCl-85º sample is formed by isolated nuclei. The tendency towards the formation of isolated nanoparticles in NaCl-85º is due to an enhancement of shadowing effects at this deposition angle. The lack of intense diffraction peaks in this sample sustains a poor crystalline order with a limited number of particles with well-defined and defect-free (200) and (220) planes parallel to the substrate surface. It also agrees with the amorphisation tendency expected for materials deposited under ballistic conditions during
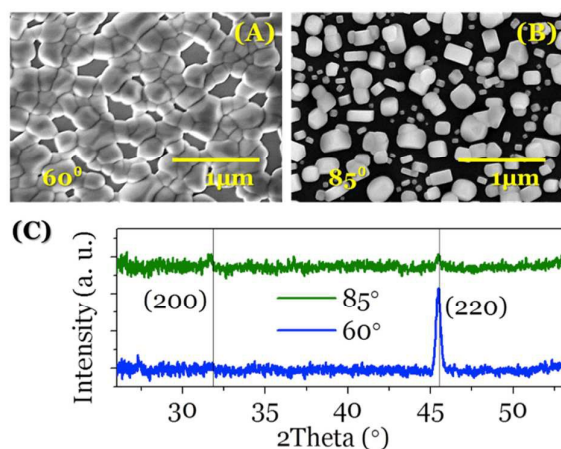
Figure 1. NaCl nanoparticles prepared by e-beam evaporation at oblique angles. (top) Normal scanning electron micrographs of samples NaCl-60º (A) and NaCl-85º (B). The X-ray diffraction diagram of these nanocrystals is reported in (C).

_____

OAD (e.g., at room temperature and oblique angles) that preclude the surface diffusion of ad-particles[34,35]. We will see later that this poor crystallization degree and/or heterogeneous crystalline character of nanoparticles may have important effects on the ripening process.

"In-situ" SEM observation of ripening

Samples were introduced in the ESEM microscope where the temperature was brought down to ca. 4º C before increasing the relative humidity up to a value close to 80% (a typical evolution of the relative humidity expressed in percentages is shown in Figure 2 D). After reaching these temperature and humidity values, the NaCl nanoparticles experienced progressive changes in shape and size that were monitored "in situ" in the microscope. These changes are evidenced by the series of successive electron micrographs (taken for ca. 15 min) shown in Figure 2 A) and the evaluation reported in Figure 2 C) of the number and size distribution of nuclei directly deduced from the images. The plots in this figure reveal a decrease of ca. one third in the number of nuclei and a clear increase from sizes smaller than 0.3 μm in the initial state (i.e., image 1 in the Figure 2A) to final situations (i.e. images 4 and 5 in Figure 2A) with a considerable number of particles between 0.2 and 0.6 μm and big crystals of up to 1.5 μm, all this meaning an increase in average size from 0.06 to 0.16 μm along the whole ripening process. This analysis also revealed that the calculated total volume of salt, determined as Nd^3 (N, number of particles in each case taken as cubic), is practically equivalent before (39000 $μm^3$) and after (33300 $μm^3$) the ripening experiment. A rough estimate of particle distribution also showed that the average distance between the edges of nanoparticles varies from an initial value D_i of 0.47 μm to D_f = 0.74 μm in the final state. The observed evolution involves the complete dissolution of some nanoparticles and the increase in size of others, both processes occurring in parallel as clearly observed in the reported images. Phenomenologically, this behaviour is typical of an Ostwald ripening mechanism where the smallest nanoparticles dissolve and their constituent material is transferred to the growing particles. As we will discuss later, in this system the ripening process may be driven by additional factors and the
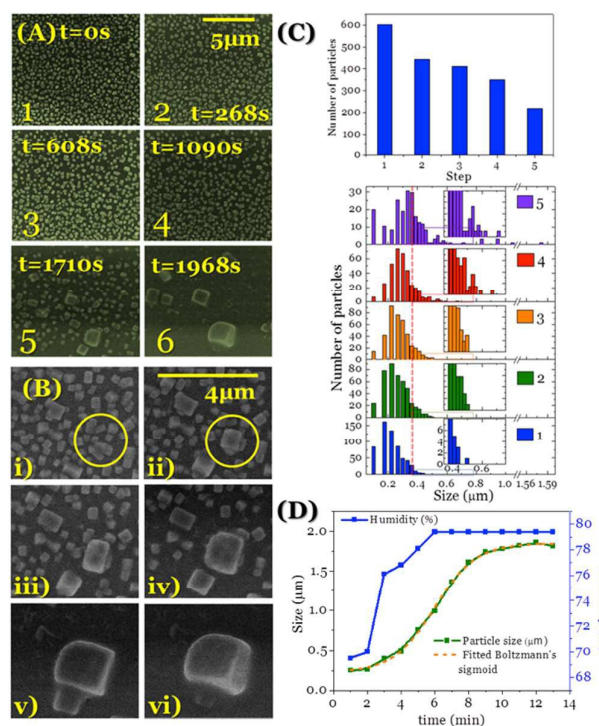

Figure 2. Evolution of the number and particle size distribution of nanoparticles in sample NaCl-85º after exposure to a humid environment. A) Normal SEM micrographs of the deposited NaCl nanoparticles taken at successive periods of time as indicated. In panel 6 water condensation accompanied by the complete dissolution of the smallest crystallites can be observed. B) Enlarged images of a selected zone monitoring the evolution of the nanoparticle reaching a maximum final size. C) Plots of the number of nanoparticles and particle size distribution as a function of exposure time to water vapour. The second inserted representations in a more expanded y-axis have been included to better visualize the evolution of the number of particles of higher sizes. D) Evolution of the water pressure in the ESEM chamber as a function of time and plot of the size evolution of the nanoparticle selected in B) (estimated from its projected area) to determine its growth kinetics. Superimposed onto the experimental curve is plotted a fitting Boltzmann's sigmoidal curve. The onset of size increase at a maximum vapor pressure of approximately 440 Pa indicates the point at which water condenses and forms a continuous water layer on the sample surface.

_____

selection of particles that grow/dissolve might not only depend on size effects as in a classical Ostwald ripening mechanism.[18]

To get a deeper insight into the kinetics of this process, we closely followed the evolution of a nucleus experiencing the largest size increase within the observation area (i.e., in this particular experiment we selected the encircled nanoparticle in Figure 2 B)). Figure 2 D) shows that the function size vs. time d(t) adopts a sigmoidal shape that can be fitted with a Sigmoidal Boltzmann Equation (SBE)[6]:

$$d(t) = \frac{d_i - d_f}{1 + e^{(t - t_i)/\Delta t}} + d_i \qquad (1)$$

where d_i and d_f are the initial and final sizes of the selected crystal, in this case taken for simplicity in one dimension as 0.23 and 1.85 μm, respectively. The parameter t_i represents the critical exposure time and corresponds to the inflexion point of the curve, i.e., for $t<t_i$ the crystal size varies at an increasingly growing rate, while for $t>t_i$ the crystal size rate decreases progressively until converging to its final size d_f. The growth period is described by Δt. In the present experiment t_i = 6.0 min and Δt= 1.2 min, meaning that the whole ripening process occurs in ca. 12 min. A reasonable assumption is that the initial induction period of 6.0 min accounts for the time required for saturating a condensed water layer with Cl^- and Na^+ ions, in other words, to dissolve the external layers of the NaCl particles up to reach steady-state ion diffusion conditions among nuclei. Within this scheme the observed increasing rate of $\Delta d(t)$ in the first part of the ripening process relates with the short average distance of D_i= 0.47 μm existing between the targeted nanoparticle and the surrounding nuclei, all of them a net source of Cl^- and Na^+ ions. In the second part of the experiment (i.e., when $t>t_i$) the area surrounding the monitored nanoparticle becomes progressively depleted from these small nuclei which are now separated by D_f= 0.74 μm, implying that the growth process slows down to finally stop. In the final stage, salt dissolution and re-deposition compensate and the overall system reaches a stationary state. A similar evolution was also found for sample NaCl-60º, although the connected microstructure of NaCl nanoparticles in this sample precluded a quantitative analysis (see supporting information S1). The basic assumption of this ripening mechanism, i.e., the migration of ions in a condensed layer of water was directly observed by Salmeron et al[23-25] in an "in situ" environmental XPS and AFM study showing the partial dissolution of alkali halide single crystals and the incorporation of their constituent ions into the liquid layer.

Crystallization and facet evolution

To a first approximation, the phenomenology of the ripening described by eq. 1 might agree with a typical Ostwald process driven by particle size differences[2,7-16], i.e., the increase in size of the bigger particles at expenses of the smallest ones that disappear. However, a closer look to the results suggests that other factors besides size effects may be involved in the process. The XRD spectra in Figure 3 A) taken for sample NaCl-60º before and after the ESEM experiments indicate that an increase in crystallization degree from an initially less crystalline state and a drastic change in nanocrystals plane texture from a (220) to a (200) preferential orientation occur in parallel to ripening. According to the schematic NaCl fcc unit cell drawings in Figure 3 C) the XRD determined textural change implies a transformation of the external facets of nanoparticles which, after water vapour exposure, would be terminated by (200) and equivalent family planes (i.e., (020) and (002)). A similar evolution was also found for sample NaCl-85º (c.f., Figure 3B)), which changed from an initial state with (200) and (220) planes parallel to the substrate (the low intensity of these peaks suggests a poor crystallinity) to a final situation where a well-defined (200) peak proves a net evolution of both crystallinity and texture. The general character of this (220) to (200) textural transformation was confirmed in an "in situ" XRD experiment at 298 K for sample NaCl-60º exposed to water saturated air in the
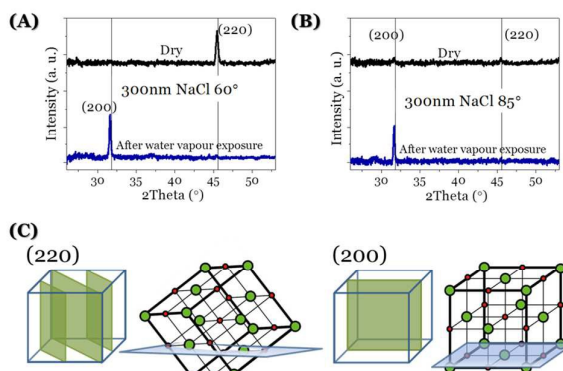

Figure 3. Evolution of crystallographic structure of NaCl nanoparticles after exposure to 80% humidity. A) X-ray diffractograms of sample NaCl-60º before and after exposure to water vapour at 8ºC in the ESEM. B) Idem for sample NaCl-85º. C) Representations of the crystal unit cell orientations of NaCl with respect to the substrate before and after exposure to water vapour.

_____

environmental chamber of the apparatus (see supporting information S2).

These crystallographic rearrangements determined by XRD run in parallel to changes in the shape and facet orientation of nanoparticles. Figures 4 A) and C) show a series of successive cross section ESEM micrographs taken for sample NaCl-60º at 40 s intervals once the ripening threshold conditions were reached. A video with the whole set of micrographs recorded during this experiment is presented as supplementary information (S3). Besides a common change in the nanoparticles shape from rounded to cubic edged form, a careful observation of selected nuclei (figure 4 B)) shows the disappearance of facets forming 45º with the substrate (in those cases where such facets can be devised in the rather rounded shapes of the initially deposited crystallites) and the progressive evolution of 90º and 180º oriented facets (i.e. perfect cubic shapes). Similar effects could be observed for sample NaCl-85º (Figure 4D). These morphological changes together with the evolution of the XRD diagrams in Figure 3, clearly demonstrate that a complete re-growing of nanoparticles occurs in parallel to their size increase by ripening.

Ripening driving forces

The experimental results summarized in Figures 1-4 require the dissolution and mobilization of Na+ and Cl- ions through a layer of water condensed on the nanoparticles and onto the free zones of the substrate that lead to a change in their number and size which, at first glance, seems to follow the surface to bulk energy premises of a classical Ostwald ripening. However, the observed changes in texture and particle shapes (i.e., facet termination) support that other factors associated with the different stabilization energies of crystals and facet termination must contribute as additional driving forces to the nanoparticles transformation and rearrangement. The
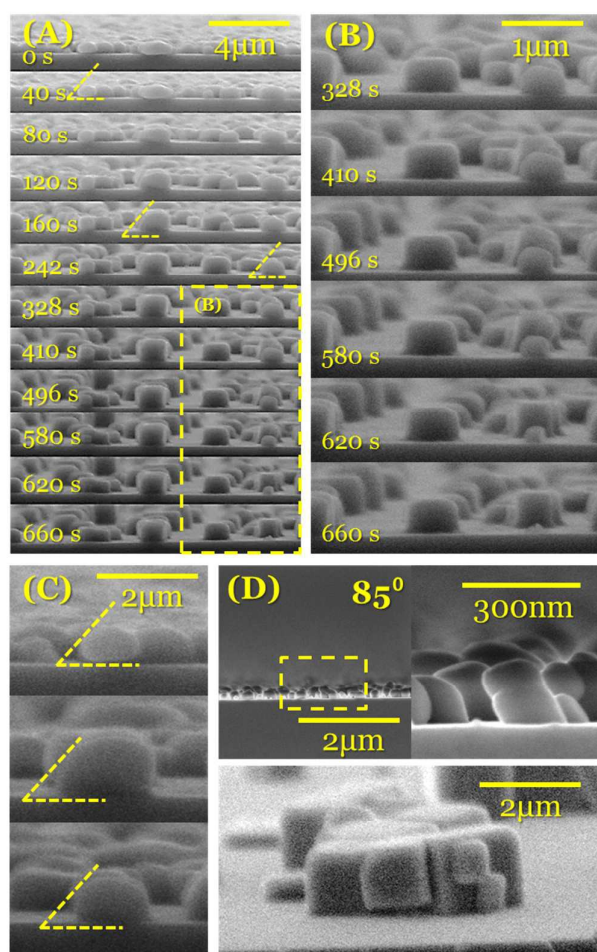
RSC Advances Accepted Manuscript

Figure 4. Shape and facet modification of NaCl nanoparticles by exposure to saturated water vapour. A) Cross section ESEM micrographs taken for sample NaCl-60º exposed to water vapour for successive periods of time as indicated. B) Enlarge views of some faceted nanoparticles. The tilted dashed lines highlight facets forming 45º with respect to the substrate. C) Enlarged views of selected nanoparticles. D) Micrographs corresponding to initial (top) and final (bottom) states taken during a similar experiment with sample NaCl-85º. A tilted morphology of the nanoparticles in the initial state is clearly visible in the enlarge micrograph in the right side.

_____

observed changes can be accounted for by the cartoons in Figure 3: in the initial sate a majority of nanoparticles orient with their (220) planes parallel to the substrate, while some of them are terminated in (200) facets forming 45º with the substrate surface. Regrowth of nanoparticles after water vapor exposure induces their rearrangement into a cubic crystalline structure with the (200) planes parallel to the substrate and a termination in crystallographic equivalent (200), (020) and (002) facets. (220) and (200) crystal faces of NaCl have ion densities36 of 4.44 and 6.29 ions nm-2 and, according to free-energy calculations by Mulheran,[36] surface energies of 160 and 267 mJ m-2 respectively (note that these values should be taken with a negative sign if referred as

Gibbs energies) [37]. This evolution of crystal facets upon ripening agrees with the classical Gibbs-Wulff postulates of equilibrium shapes of crystal growth (NaCl crystals are known to terminate in 100 facets) rather than with the Frank-Chernov principles of steady-state growth shapes[38].

Besides particle size and facet termination, the partial amorphous character of the NaCl nuclei prepared by OAD must operate as an additional driving force of nanoparticle transformation and ripening. In fact, as suggested by the XRD analysis of sample NaCl-85º, nanoparticle ripening is accompanied by a net increase in crystallization degree suggesting that more amorphous particles dissolve preferentially and/or that a partial dissolution and precipitation in more crystalline form is also occurring in the growing particles. It is worth noting that a consequence of this behaviour is that the nanoparticles experiencing ripening are not necessarily those having a bigger size but those which might be better crystallized in the "as deposited" state or a combination of both factors. Unfortunately, this point could not be assessed during the "in-situ" SEM and global XRD experiments carried out in this work. Overall, these evidences design a complex situation where the surface to bulk energy ratio commonly taken as the effective driving force of a classical Ostwald ripening process, must be complemented with differences in facets energies and between partially amorphous and well crystallized OAD NaCl nanoparticles. Similar considerations have been claimed to explain differences in vaporization temperatures of NaCl nanocrystals depending on their size[39]. The implications of these findings can be of relevance to account for recrystallization and ripening phenomena in natural environments[20–22] or in harsh conditions or even in space[40] where partial amorphisation or unfavourable termination of small nanoparticles could provoke their spontaneous transformation under conditions enabling mass transport and particle re-growth.

Experimental

NaCl nanoparticles were deposited on a silicon (100) wafer by electron beam evaporation of pellets of this material (Sigma Aldrich). The substrates were placed at 60º and 85º oblique angles with respect to the evaporation source and separated from it by approximately 0.8 m. The deposition process was controlled with a calibrated quartz crystal monitor. For the reported experiments, 150 nm and 26 nm equivalent thickness of NaCl were selected for samples NaCl-60º and NaCl-85º, respectively.

Specimens were placed in an ESEM where both the water vapor pressure and the temperature were adjusted to induce condensation while successively taking normal and cross section micrographs, these latter after dicing the silicon substrates. The same specimens were also examined by XRD in a Bragg-Brentano configuration before and after their low temperature exposure to water vapour in the ESEM chamber. In parallel, we carried out an "in situ" XRD analysis with an environmental cell where the original sample was exposed at room temperature to water vapour at saturated conditions. The ESEM experiments were carried out in a FEI Quanta 250 FEG system working at 5 kV at a working distance of 6mm from the surface. Precautions were taken to minimize any possible

ARTICLE

effect of the electron beam on the ripening process and adjustments were made in the dosage of electrons and scanning rate. Images were taken while increasing the vapour pressure into the chamber and by adjusting their temperature with a Peltier device. Number of particles and average inter-particle distance and size has been determined by directly analysing the images using ImageJ, a National Institutes of Health (NIH)–sponsored image processing platform (www.ini.uzh.ch/~acardona/trakem2.html).

X-ray diffraction diagrams in a Bragg-Brentano configuration were taken in a D8 Discover diffractometer (Bruker AXS). In-situ XRD recrystallization experiments at room temperature upon exposure to saturated vapor pressure conditions at room temperature were carried out in a X'Pert Pro from Panalytical for X-ray angles < 1 °.

After preparation and during the transfer of samples from the ESEM to the XRD chambers the samples were kept in a desiccator to avoid possible effects of the humidity of the atmosphere. The stability of the samples during their manipulation in air for the introduction in the ESEM or XRD chambers was checked by successive observations in a conventional SEM microscope.

Acknowledgements

References

1   H. Furedi-Milhofer, *Pure Appl. Chem.* 1981, **53** (11)
2   R. Boistelle, J. Astier, *J. Cryst. Growth* 1988, **90**, 14
3   S.C. Jain, A.E. Hughes, *J. Mater. Sci.* 1978, **13**, 1611
4   K. Glasner, F. Otto, T. Rump, D. Slepčev, Eur. *J. Appl. Math.* 2009, **20**, 1
5   I.C.K. Karl Glasner, *Interfaces Free Boundaries* 2009, 37.
6   S.K. Hait, S.P. Moulik, R. Palepu, R. *Langmuir* 2002, **18**, 2471.
7   F. Wang, V.N. Richards, S.P. Shields, W. E. Buhro, *Chem. Mater.* 2014, **26**, 5.
8   I. Lifshitz, V. Slezov, *Sov. Phys. Jetp-Ussr* 1959, **8**, 331.
9   I. Lifshits, V. Slezov, *Sov. Phys.-Solid State* 1960, **1**, 1285.
10 I. Lifshitz, V.V. Slyozov, *J. Phys. Chem. Solids* 1961, **19**, 35.
11 C. Wagner, *Z. Elektrochem.* 1961, **65**, 581.
12 J.H. Yao, K.R. Elder, K. H. Guo, M. Grant, *Phys. Rev. B* 1993, **47**, 14110.
13 M. Iggland, M. Mazzotti, *Cryst. Growth Des.* 2012, **12**, 1489.
14 T. Vetter, M. Iggland, D.R. Ochsenbein, F.S. Hänseler, M. Mazzotti, *Cryst. Growth Des.* 2013, **13**, 4890.
15 L. Ratke, P.W. Voorhees, *Growth and Coarsening: Ostwald Ripening in Material Processing*; Springer Science & Business Media, 2002.
16 H. Chun Zeng, *Curr. Nanosci.* 2007, **3**, 177.
17 K. Biswas, K.; N. Varghese, N.; C.N.R. Rao, *J. Mater. Sci. Technol.* 2009, **24**, 615.
18 W. Ostwald, W. *Studien Über Die Bildung Und Umwandlung Fester Körper. 1. Abhandlung: Übersättigung Und Überkaltung.* 1897.
19 J.S. Jahren, *Clay Miner.* 1991, **26**, 169.
20 J. Warren, *Earth-Sci. Rev.* 2000, **52**, 1.
21 M. Angeli, J.P. Bigas, D. Benavente, B. Menéndez, R. Hébert, ¡ C. David, *Environ. Geol.* 2006, **52**, 205.
22 M.E. Wise, K. Baustian, T. Koop, M. A. Freedman, E.J. Jensen, M.A. Tolbert, *Atmospheric Chem. Phys.* 2012, **12**, 1121.
23 M. Salmeron, A. Verdaguer, J.J. Segura, J. Fraxedas, H. Bluhm, *J. Phys. Chem. C* 2008, **112**, 16898.
24 K. Arima, P. Jiang, D.S. Lin, A. Verdaguer, M. Salmeron, *J. Phys. Chem. A* 2009, **113**, 9715.
25 K. Arima, P. Jiang, X. Deng, H. Bluhm, M. Salmeron, *J. Phys. Chem. C* 2010, **114**, 14900.
26 K. Yagi, G. Honjo, *J. Phys. Soc. Jpn.* 1964, **19**, 1892.
27 M.M. Hawkeye, M.T. Taschuk, J.M. Brett, *Glancing Angle Deposition of Thin Films*; John Wiley & Sons, Ltd, 2014.
28 A.Barranco, A. Borras, A.R. Gonzalez-Elipe, A. Palmero, *Progr. Mater. Sci.* DOI 10.1016/j.pmatsci.2015.06.003.
29 L.G. Schulz, *J. Chem. Phys.* 1949, **17**, 1153.
30 H. Bethge, K.W. Keller, *J. Cryst. Growth* 1974, **23**, 105.
31 J. Yang, R. Dariani, C. Elliott, C. Buzea, K. Robbie, *Soc. Vac. Coat. 49th Annual Technical Conference Proceedings* 2006, (505/856-7188) 689.
32 Y. He, Y. Zhao, *Nanoscale* 2011, **3**, 2361.
33 L. González-García, J. Parra-Barranco, J.R. Sánchez-Valencia, A. Barranco, A. Borras, A.R. Gonzalez-Elipe, M.C. García-Gutierrez, J. J. Hernandez, D. R. Rueda, T.A. Ezquerra *Nanotechnology* 2012, **23**, 205701.
34 T. Karabacak, J.P. Singh, Y.P. Zhao, G.C. Wang, T.M. Lu, *Phys. Rev. B* 2003, **68**, 125408.
35 A. Amassian, K. Kaminska, M. Suzuki, L. Martinu, K. Robbie, *Appl. Phys. Lett.* 2007, **91**, 173114.
36 D.R. Lide, *CRC Handbook of Chemistry and Physics*, Internet Version (CRC Press: Boca Raton, FL, 2005; section 4, pp 160. http://www.hbcpnetbase.com)
37 P.A. Mulheran,. *Model. Simul. Mater. Sci. Eng.* 1994, **2**, 1123.
38 P. Dandekar, Z.B. Kuvadia, M.F. Doherty, *Annu. Rev. Mater. Res*. 2013, **43**, 359.
39 N. Kana, S. Khamlich, J.B.K. Kana, M. Maaza, *Surf. Rev. Lett.* 2013, **20** (01).
40 J.W. Mullin, *Crystallization*. Butterworth-Heinemann, Oxford, ed. 4, 2001, pp. 193

RSC Advances Accepted Manuscript